Complete characterization of a coherent superposition of atomic states by asymmetric attosecond photoionization

Candong Liu* and Mauro Nisoli

Department of Physics, Politecnico di Milano, National Research Council of Italy, Institute of Photonics and Nanotechnologies (CNR–IFN), Piazza L. da Vinci 32, 20133 Milano, Italy

(Received 28 March 2012; published 29 May 2012)

A method for the complete characterization of a coherent superposition of atomic states, prepared by a pump pulse, is presented. The technique is based on the measurement of two asymmetry parameters, related to the photoionization of the generated electron wave packet by isolated attosecond pulses. By numerically solving the fully three-dimensional time-dependent Schrödinger equation, it is demonstrated that the temporal evolution of the population of the atomic states involved in the coherent superposition can be mapped onto the amplitude-modulated asymmetry in the direction of the attosecond probe pulse polarization. The results of the numerical simulations show that it is possible to achieve a unique determination of static and time-dependent populations by measuring only a few ionization asymmetry parameters.

DOI: 10.1103/PhysRevA.85.053423 PACS number(s): 32.80.Rm, 42.65.Ky, 42.65.Re

I. INTRODUCTION

According to the laws of quantum mechanics the motion of an electron in atoms and molecules corresponds to the temporal evolution of a coherent superposition of stationary states. In the simplest case of two states, the corresponding electron density oscillates with a period $T = 2\pi/\Delta\mathcal{E}$, where $\Delta\mathcal{E}$ is the energy difference between the two states (atomic units will be used in the work: $e = \hbar = m_e = 1$, where e and m_e are the electron charge and mass, respectively). The corresponding temporal scale ranges from microseconds, in the case of Rydberg states, to a few attoseconds. The measurement of this electronic motion in atoms and molecules is an important topic in attosecond science [1,2]; various experimental techniques have been proposed and partly implemented. The modulation of the spectrum of attosecond pulses produced from single-electron recollision gives an insight into the wave-packet motion [3]. Attosecond transient absorption spectroscopy has been successfully applied to real-time observation of valence electron motion in krypton ions [4,5]. In this case a sub-4-fs, near-infrared pulse generates a coherent superposition of two spin-orbit split states of the $4p$ subshell of Kr^+. An attosecond probe pulse subsequently promotes the system into a common final state. The quantum interference gives rise to a temporal modulation of the transition probability, which allows one to reconstruct the valence-shell wave-packet motion. A different method is based on the measurement of the asymmetry in the photoionization of the coherent superposition of states by attosecond pulses as a function of the delay between the pump pulse, which prepares the coherent superposition, and the probe extreme ultraviolet (XUV) pulse [6–10]. The temporal evolution of the asymmetry allows one to monitor the electron motion in atoms and molecules. The effects of few-cycle attosecond pulses on ionized electron momentum and energy spectra have been analyzed by Peng *et al.* [11].

In order to achieve a complete characterization of the bound-electron wave packet, corresponding to the coherent superposition of states, it is required to measure both the populations of the states involved in the coherent superposition and the time-dependent phase shift. Various mechanisms, such as electron-electron interactions, can give rise to a loss of coherence, which leads to a temporal evolution of the population of the states. For this reason, a precise measurement of the population of the states might give access to the investigation of relevant multielectron dynamics. The role of the population of the coherently coupled states on the photoionization process induced by the attosecond probe pulses has never been discussed, to our knowledge. In this work, we investigate the attosecond photoionization process in a model hydrogen atom prepared in a superposition of $1s$ and $2p_0$ stationary states with several different populations. The photoionization asymmetry parameter in the direction of the field polarization is calculated as a function of the delay between the pump and probe pulses by numerically solving the fully three-dimensional time-dependent Schrödinger equation (3D-TDSE), which allows one to retrieve crucial information about the role of the population in the photoionization of the bound-electron wave packet generated by the pump pulse. In particular, the effect of the population on the amplitude of the asymmetry curve is discussed. A method is proposed to uniquely determine the population of a coherently coupled state based on the measurement of a second asymmetry parameter, which takes into account the electrons emitted in the direction perpendicular to the probe field polarization. By taking a simple example, we further demonstrate that this approach can be extended to the measurement of the time-dependent population.

II. THEORETICAL MODEL AND NUMERICAL METHODS

In order to reveal the essentials of our approach, we concentrate on a theoretically tractable example, i.e., a hydrogen atom prepared by a pump pulse in a superposition of $1s$ and $2p_0$ stationary states characterized by atomic orbitals $\psi_{1s}(\mathbf{r})$ and $\psi_{2p_0}(\mathbf{r})$. The prepared wave function can be expressed as

$$\psi(\mathbf{r},t) = \sqrt{P_{1s}}\,\psi_{1s}(\mathbf{r}) + \sqrt{1-P_{1s}}\,e^{i\gamma(t)}\,\psi_{2p_0}(\mathbf{r}), \quad (1)$$

*cdliu@siom.ac.cn

where P_{1s} is the population of the $1s$ state and $\gamma(t) = \Delta\mathcal{E}t + \phi$ is the time-dependent phase shift corresponding to the electron motion with a period $T = 2\pi/\Delta\mathcal{E}$. P_{1s} and ϕ depend on the excitation scheme. The interaction between atomic systems and external intense laser fields is governed by the TDSE. In the single-active-electron (SAE) approximation and the Cartesian spherical coordinates, the fully 3D-TDSE is described as

$$i\frac{\partial}{\partial t}\psi(\mathbf{r},t) = \left[-\frac{1}{2}\frac{1}{r^2}\frac{\partial}{\partial r}r^2\frac{\partial}{\partial r} + \frac{\hat{\ell}^2}{2r^2} + V(r) + V_I(\mathbf{r},t)\right]\psi(\mathbf{r},t), \tag{2}$$

where $V(r)$ is an effective Coulomb potential with a spherical symmetry, $\hat{\ell}^2$ is the square of the orbit angular momentum operator, and $V_I(\mathbf{r},t)$ is the Hamiltonian for the atom interacting with the applied laser field. In the case of a hydrogen atom the atomic potential is given by $V(r) = -1/r$. In the length gauge and in the dipole approximation, the interaction Hamiltonian for the hydrogen atom ionized by an isolated attosecond pulse with a linear polarization along the z axis can therefore be written as $V_I(\mathbf{r},t) = -z[dA_z(t)/dt]$. Here the vector potential $A_z(t)$ used to define the Gaussian attosecond pulse is given by

$$A_z(t) = -\frac{\sqrt{I_0}}{\omega_0}\, e^{-2\ln 2(t^2/\tau_d^2)}\, \sin(\omega_0 t + \varphi_0), \tag{3}$$

where I_0, ω_0, τ_d, and φ_0 are the peak intensity, the central angular frequency, the pulse duration, and the initial carrier envelope phase, respectively. Upon using an expansion of $\psi(\mathbf{r},t)$ in a series of partial waves indexed by angular quantum number ℓ and magnetic quantum number m as

$$\psi(\mathbf{r},t) = \sum_{\ell=0}^{\infty}\sum_{m=-\ell}^{\ell}\frac{1}{r}\,\varphi_{\ell,m}(r,t)Y_\ell^m(\theta,\phi), \tag{4}$$

Eq. (2) reduces to a set of coupled equations between the different channels $\ell-1$, ℓ, and $\ell+1$ for the radial wave function $\phi_{\ell,m}(r,t)$ [12,13]:

$$i\frac{\partial}{\partial t}\varphi_{0m}(r,t) = \left[-\frac{1}{2}\frac{\partial^2}{\partial r^2} + V(r)\right]\varphi_{0m}(r,t) - c_{1m}r\frac{dA_z(t)}{dt}\varphi_{1m}(r,t) \tag{5}$$

for $\ell = 0$ and, for $\ell > 0$,

$$i\frac{\partial}{\partial t}\varphi_{\ell m}(r,t) = \left[-\frac{1}{2}\frac{\partial^2}{\partial r^2} + \frac{\ell(\ell+1)}{2r^2} + V(r)\right]\varphi_{\ell m}(r,t) - r\frac{dA_z(t)}{dt}[c_{\ell,m}\varphi_{\ell-1,m}(r,t) + c_{\ell+1,m}\varphi_{\ell+1,m}(r,t)]. \tag{6}$$

Here $c_{\ell,m}$, which is related to the Clebsch-Gordan coefficient, is given by

$$c_{\ell,m} = \sqrt{\frac{(\ell-m)(\ell+m)}{(2\ell-1)(2\ell+1)}}. \tag{7}$$

It is worth mentioning that those partial waves with different magnetic quantum numbers cannot be coupled together because the angular momentum component along the z axis is conserved for the use of linearly polarized attosecond pulses. The radial wave function $\varphi_{\ell m}(r,t)$ is discretized at the uniform grids with a spacing of δr, i.e., $r_i = i\delta r$, where $i = 1,2,\ldots,N-1$. In the evolution of the time-dependent wave function, the radial space is truncated at $r_{\max} = N\delta r$, which should be large enough to completely cover the wave function diffusion and to avoid the reflection of the wave function at the outer boundary. We employed the five-point central finite-difference (FD) scheme to approximate the second derivative $\partial^2/\partial r^2$ in Eqs. (5) and Eq. (6) [14]. At the grid points away from $r_1 = \delta r$, the FD representation of the operator $\partial^2/\partial r^2$ is given by

$$\left.\frac{\partial^2\varphi_{\ell m}(r,t)}{\partial r^2}\right|_{r=r_i} = \frac{1}{12(\delta r)^2}[-\varphi_{\ell m}(r_i-2\delta r,t) + 16\varphi_{\ell m}(r_i-\delta r,t) - 30\varphi_{\ell m}(r_i,t) + 16\varphi_{\ell m}(r_i+\delta r,t) - \varphi_{\ell m}(r_i+2\delta r,t)] \quad (1 < i < N). \tag{8}$$

At the smallest grid point $r_1 = \delta r$, the FD representation of the operator $\partial^2/\partial r^2$ is slightly different and can be expressed as

$$\left.\frac{\partial^2\varphi_{\ell m}(r,t)}{\partial r^2}\right|_{r=\delta r} = \frac{1}{12(\delta r)^2}[-30\varphi_{\ell m}(\delta r,t) + 16\varphi_{\ell m}(2\delta r,t) - \varphi_{\ell m}(3\delta r,t) - C\varphi_{\ell m}(\delta r,t)], \tag{9}$$

which refers to a correction factor C chosen to faithfully reproduce the ground-state energy of the target atom [14]. We point out that the value of C is dependent on δr. The temporal evolution of the wave function is carried out by a Krylov subspace decomposition scheme based on the Arnoldi algorithm [15,16] under the boundary conditions $\varphi_{lm}(r = 0,t) = 0$ and $\varphi_{lm}(r_{\max},t) = 0$.

The probability amplitude of the ionized electron with momentum $\mathbf{p} = (p,\theta_p,\phi_p)$ is obtained by the projection of the final wave function onto the field-free Coulomb continuum state $\psi_{\mathbf{p}}^C(\mathbf{r})$ [17,18]:

$$a(\mathbf{p}) = \left\langle\psi_{\mathbf{p}}^C(\mathbf{r})\middle|\psi(\mathbf{r},t_f)\right\rangle. \tag{10}$$

For the hydrogenlike atom with an attractive potential $V(r) = -Z/r$, the quantum scattering theory gives the expansion of $\psi_{\mathbf{p}}^C(\mathbf{r})$ as [11]

$$\psi_{\mathbf{p}}^C(\mathbf{r}) = \frac{1}{(2\pi)^{3/2}}\frac{4\pi}{pr}\sum_{\ell=0}^{\infty}\sum_{m=-\ell}^{\ell} i^\ell e^{i\sigma_\ell}\mathcal{F}_\ell\left(-\frac{Z}{p},pr\right) \times Y_\ell^m(\theta,\phi)\, Y_\ell^{m*}(\theta_p,\phi_p), \tag{11}$$

where Z is the net nuclear charge, $\sigma_\ell = \arg\Gamma(\ell+1+i\frac{Z}{p})$ is the Coulomb phase shift, and $\mathcal{F}_\ell(\eta,\rho)$ is the Coulomb wave function, which is given in terms of confluent hypergeometric function by

$$\mathcal{F}_\ell(\eta,\rho) = \frac{2^\ell e^{-\pi\eta/2}|\Gamma(\ell+1+i\eta)|}{\Gamma(2\ell+2)} \times \rho^{\ell+1}e^{-i\rho}{}_1F_1(\ell+1-i\eta;2\ell+2;2i\rho). \tag{12}$$

We point out that $\mathcal{F}_\ell(\eta,\rho)$ is a real function. By substituting Eqs. (4) and (11) in Eq. (10), we have

$$a(p,\theta_p,\phi_p) = \sqrt{\frac{2}{\pi}} \sum_{\ell=0}^{\infty} \sum_{m=-\ell}^{\ell} (-i)^\ell e^{-i\sigma_\ell} Y_\ell^m(\theta_p,\phi_p) \times \frac{1}{p} \int_0^{+\infty} \mathcal{F}_\ell\left(-\frac{Z}{p}, pr\right) \varphi_{\ell m}(r,t_f) dr, \quad (13)$$

which is the main formula used to calculate the photoelectron momentum distribution in this work. In the practical calculation the angular quantum number is truncated at $\ell_{\max}$, which is set to assure that the contribution from those partial waves with $\ell > \ell_{\max}$ can be neglected. By making use of $a(p,\theta_p,\phi_p)$, the triple differential ionization probability (TDIP), which represents the probability density of the photoelectron with momentum $\mathbf{p} = (p,\theta_p,\phi_p)$, can be expressed as

$$T(\mathcal{E},\theta_p,\phi_p) = \frac{\partial^3 P}{\partial \mathcal{E} \sin\theta_p \partial\theta_p \partial\phi_p} = \sqrt{2\mathcal{E}} |a(\sqrt{2\mathcal{E}},\theta_p,\phi_p)|^2, \quad (14)$$

where $\mathcal{E} = p^2/2$ is the kinetic energy of photoelectron.

Since the coupled wave function is axially symmetric with respect to the z axis, the TDIP is independent of ϕ_p. The integration of TDIP over energy $\mathcal{E}$ defines the polar-dependent probability density:

$$P(\theta_p) = 2\pi \int_0^{+\infty} T(\mathcal{E},\theta_p,0) d\mathcal{E}. \quad (15)$$

The normalized asymmetry A_1 in the direction of the XUV pulse polarization is therefore given by

$$A_1 = \frac{P(0) - P(\pi)}{P(0) + P(\pi)}. \quad (16)$$

The parallel-perpendicular asymmetry A_2 is defined by

$$A_2 = \frac{P(0) + P(\pi) - 2P(\pi/2)}{P(0) + P(\pi) + 2P(\pi/2)}, \quad (17)$$

which represents the difference of the photoelectron emission parallel and perpendicular to the direction of the XUV pulse polarization.

The simulation parameters used in our calculation are the following: the radial grid spacing is $\delta r = 0.02$ a.u., the maximum radial distance is $r_{\max} = 300$ a.u., the maximum angular quantum number is $l_{\max} = 10$, the time step of wave function propagation is $\delta t = 0.01$ a.u., the Arnoldi propagation order is $M = 50$, and the correction factor in Eq. (9) is $C = -1.04081$, which leads to the H atom ground-state energy $E_0 = -13.6057$ eV. We have chosen the values of the parameters $r_{\max}$ and $l_{\max}$ using the following criterion: all the calculated physical quantities, such as the normalized asymmetries, have to converge to the same value upon variations of the two parameters with respect to the chosen values.

III. RESULTS AND DISCUSSION

We consider a coherent superposition of the $1s$ and $2p_0$ stationary states of a hydrogen atom, produced by a pump pulse. The generated electron wave packet depends on the

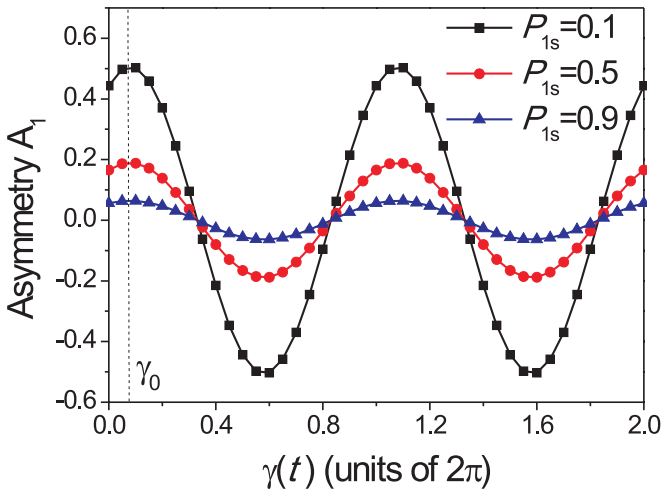

FIG. 1. (Color online) Normalized asymmetry A_1 in the direction of the probe pulse polarization as a function of the phase shift $\gamma(t)$, calculated for three different populations P_{1s} of the $1s$ state: $P_{1s} = 0.1$ (black squares), $P_{1s} = 0.5$ (red dots), and $P_{1s} = 0.9$ (blue triangles). Probe pulse parameters used in the calculation are duration of 130 as, central photon energy of 36 eV, and peak intensity $I_0 = 1 \times 10^{12}$ W/cm^2.

population P_{1s} of the $1s$ state and on the phase shift $\gamma(t)$. Note that different $\gamma(t)$ correspond to different pump-probe temporal delays. We have first calculated the photoelectron momentum distribution for the coupled state ionized by a 130-as pulse with a central photon energy of 36 eV and a peak intensity $I_0 = 1 \times 10^{12}$ W/cm^2. Figure 1 shows the normalized asymmetry parameter A_1 as a function of phase shift $\gamma(t)$, calculated for three different populations P_{1s}. In agreement with the results reported by Yudin *et al.* [6], A_1 turns out to be an oscillating function of $\gamma(t)$ with a period $\Delta\gamma = 2\pi$. Since the bound state is projected into the continuum by the broadband XUV pulse, the oscillation of the asymmetry curve in fact provides a direct observation of the electron motion with

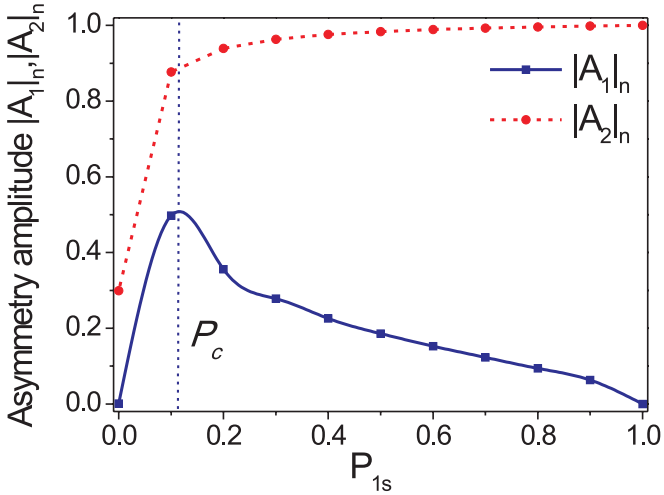

FIG. 2. (Color online) Amplitudes of the A_1 (squares) and A_2 (dots) asymmetry parameters as a function of the population P_{1s}, calculated at $\gamma(t) = \gamma_n = 2\pi(\gamma_0 + n/2)$ ($n = 0,1,2,\ldots$). The probe pulse parameters are the same as in Fig. 1.

a period $T = 2\pi/\Delta\mathcal{E}$. While the positions of the maxima and minima of A_1 are completely independent on the population, the amplitude of the asymmetry $|A_1(P_{1s})|_n$ exhibits a strong population dependence; $|A_1(P_{1s})|_n$ is the asymmetry parameter calculated at $\gamma(t) = \gamma_n = 2\pi(\gamma_0 + n/2)$, $n = 0,1,2,\ldots$, corresponding to the position of the peaks and valleys of A_1. Therefore, from an experimental point of view, in order to have a clear measurement of the electron motion, the pump pulse parameters have to be carefully set to adjust in the proper way the population of the states. This dependence suggests the possibility to extract information about the population from the measurement of the asymmetry parameter A_1.

Figure 2 shows the evolution of the asymmetry amplitude $|A_1(P_{1s})|_n$ as a function of the population P_{1s}. The asymmetry amplitude shows a nonmonotonic behavior, with a maximum at a particular population value P_c. For this reason the measurement of A_1 does not provide a unique determination of the population of the coherently coupled states. The same asymmetry amplitude can be obtained in the case of two different populations P_{1s}, one smaller than the critical population P_c and the second larger than P_c. In order to obtain a unique determination of the population we propose to measure the asymmetry parameter A_2, defined by Eq. (17). The red dashed curve in Fig. 2 displays $|A_2(P_{1s})|$ calculated at $\gamma = \gamma_n$ [hereafter referred to as $|A_2(P_{1s})|_n$] as a function of P_{1s}. The curve is a monotonic function in the whole population range. Due to the very small slope of the curve for $P_{1s} > P_c$, it is not possible to determine the population with the required accuracy by measuring only A_2. Both asymmetry parameters have to be used to obtain a precise estimation of the population. The procedure is the following: (i) the asymmetry parameter $|A_2(P_{1s})|_n$ is used to deduce if P_{1s} is smaller or larger than the critical population P_c; (ii) the asymmetry amplitude $|A_1(P_{1s})|_n$ is then used for the fine determination of the population.

We then investigated how the intensity and duration of the XUV probe pulse affect the measurement of the population. Figures 3(a) and 3(b) show $|A_2(P_{1s})|_n$ and $|A_1(P_{1s})|_n$, respectively, as a function of P_{1s}, calculated in the case of four different durations of the probe pulse, ranging from 100 to 190 as, at a peak intensity $I_0 = 1 \times 10^{12}$ W/cm^2. While $|A_2(P_{1s})|_n$ is only slightly affected by the probe pulse duration, $|A_1(P_{1s})|_n$ increases upon decreasing the pulse duration, as expected from the physical origin of the photoelectron asymmetry. Indeed, as pointed out by Yudin *et al.* [6], the asymmetry in photoelectron emission is due to the interference between the spectra of the photoelectron emitted by the two states of the coherent superposition. The interference is visible only when the probe pulse is shorter than the oscillation period, so that the two photoelectron spectra overlap, and the visibility increases upon increasing the bandwidth of the probe pulse. Therefore, depending on the value of the oscillation period, the use of ultrashort XUV pulses is strongly required since, as shown in Fig. 3(b), the $|A_1(P_{1s})|_n$ curve becomes steeper upon decreasing the probe pulse duration, thus leading to an increase of the accuracy in the measurement of the population. It is noteworthy that in order to estimate the population it is also required to measure the probe pulse duration. We have then verified that both asymmetry parameters are

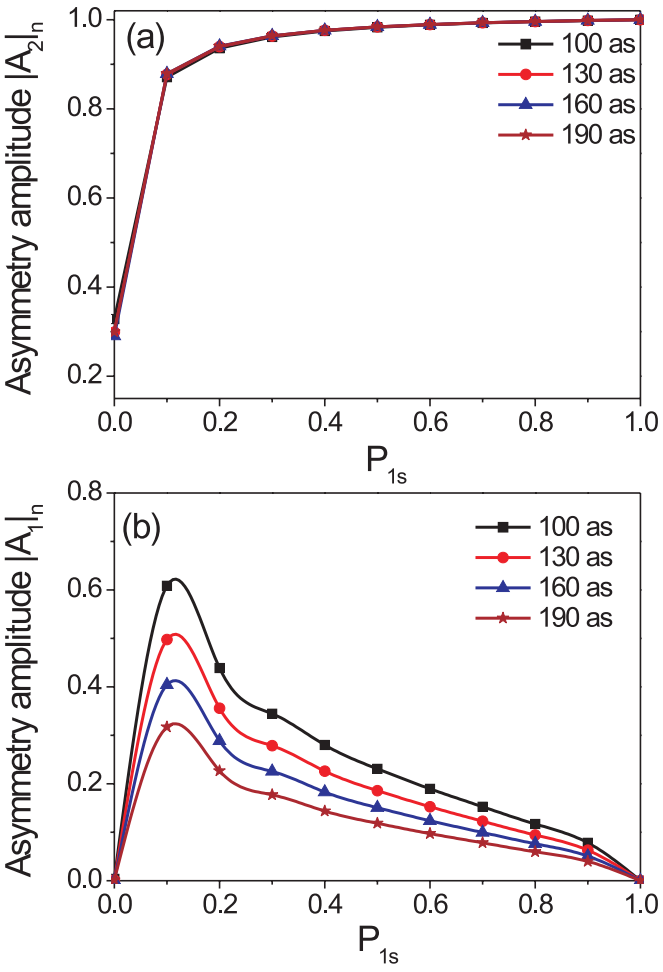

FIG. 3. (Color online) Amplitudes of the (a) A_2 and (b) A_1 asymmetry parameters as a function of the population P_{1s}, evaluated at $\gamma(t) = \gamma_n = 2\pi(\gamma_0 + n/2)$ $(n = 0,1,2,\ldots)$ in the case of four durations of the XUV probe pulse: 100 as (squares), 130 as (dots), 160 as (triangles), and 190 as (stars), with a fixed peak intensity $I_0 = 1 \times 10^{12}$ W/cm^2.

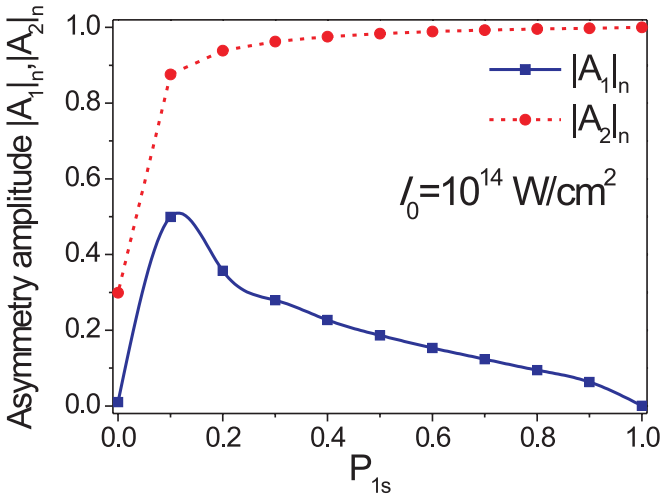

FIG. 4. (Color online) Amplitudes of the A_1 (squares) and A_2 (dots) asymmetry parameters as a function of the population P_{1s}, evaluated at $\gamma(t) = \gamma_n = 2\pi(\gamma_0 + n/2)$ $(n = 0,1,2,\ldots)$ in the case of a 130-as probe pulse with peak intensity $I_0 = 1 \times 10^{14}$ W/cm^2.

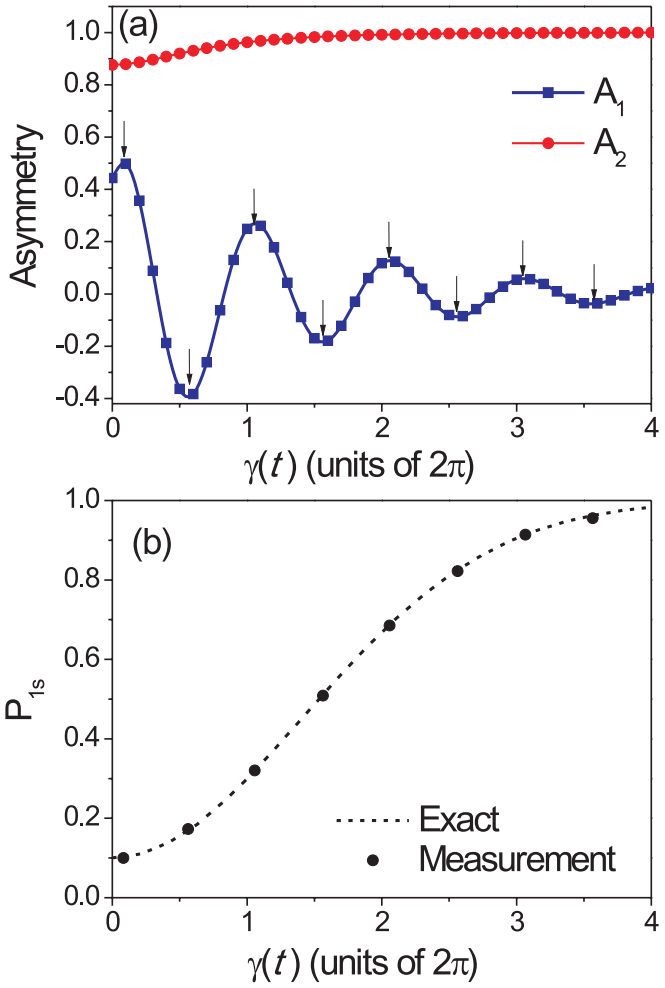

FIG. 5. (Color online) (a) Asymmetry parameters A_1 (squares) and A_2 (dots) as a function of the phase shift $\gamma(t)$, calculated for the time-dependent population $P_{1s} = 1 - 0.9e^{-(\gamma/4\pi)^2}$ ($\gamma > 0$). (b) Comparison of the exact time-dependent population (dashed line) with the corresponding reconstructions (dots). The probe pulse parameters are the same as in Fig. 1.

almost independent from the peak intensity of the probe pulse. Indeed, Fig. 4 shows $|A_1(P_{1s})|_n$ and $|A_2(P_{1s})|_n$ as a function of P_{1s}, calculated in the case of 130-as probe pulses with a peak intensity $I_0 = 1 \times 10^{14}$ W/cm^2, two orders of magnitude larger than the probe intensity assumed in the case of Fig. 2: the results obtained in the two cases are almost indistinguishable. This is an important advantage because the intrinsic relationship between the population and the asymmetry can be obtained without measuring the intensity of the attosecond probe pulse, which is often difficult to measure in the experiment.

The approach based on the measurement of the asymmetry parameters A_1 and A_2 for the determination of the population of coupled states can be also extended to monitor the temporal evolution of the population. Let us assume that the population P_{1s} is characterized by the following temporal evolution:

$$P_{1s}(\gamma) = 1 - 0.9e^{-(\gamma/4\pi)^2}, \tag{18}$$

with $\gamma > 0$. Upon scanning the phase shift $\gamma(t)$, i.e., the pump-probe time delay, the attosecond photoionization is then calculated by the exact solution of the 3D-TDSE, and the results are shown in Fig. 5(a), which displays the asymmetry parameters A_1 and A_2 as a function of $\gamma(t)$. The important feature of the A_1 curve is the periodic oscillation, which is a result of the electron motion in the coupled states, with a time-dependent amplitude, which contains the information about the temporal evolution of the population. To measure the time-dependent population, we select the asymmetry parameters at those positions where the A_1 curve reaches the peak and the valley, as denoted by the arrows in Fig. 5(a). These selected values are compared with Fig. 2, which is the intrinsic relationship between population and amplitude. Consequently, we can obtain the measured population P_{1s} as a function of $\gamma(t)$. The measured result (dots) is shown in Fig. 5(b), together with the exact time-dependent population (dashed line) obtained from Eq. (18). The excellent agreement demonstrates that this approach can be successfully extended to the measurement of a time-dependent population.

IV. CONCLUSIONS

We investigated the attosecond photoionization of a model hydrogen atom prepared by a pump pulse in a coherently coupled state, consisting of the $1s$ and $2p_0$ atomic orbitals, by numerically solving the fully 3D-TDSE. In particular, we investigated the role of the population of the states on the photoionization asymmetry. It was found that the amplitude of asymmetry in the direction of the probe polarization exhibits a strong dependence on the population of the states. A unique determination of the population of the coupled states can be achieved only by measuring a second asymmetry parameter, which takes into account also the electrons emitted in a direction perpendicular to the probe polarization direction. The same method can be also applied in the case of time-dependent populations.

ACKNOWLEDGMENTS

This research was supported by the European Research Council under the European Community's Seventh Framework Programme (FP7/2007-2013)/ERC Grant Agreement No. 227355 ELYCHE, the European Union under Contract No. 228334 JRA-ALADIN (Laserlab Europe II), and the MC-RTN ATTOFEL (FP7-238362).

[1] F. Krausz and M. Ivanov, Rev. Mod. Phys. **81**, 163 (2009).
[2] M. Nisoli and G. Sansone, Prog. Quantum Electron. **33**, 17 (2009).
[3] H. Niikura, D. M. Villeneuve, and P. B. Corkum, Phys. Rev. Lett. **94**, 083003 (2005).
[4] E. Goulielmakis, Z. Loh, A. Wirth, R. Santra, N. Rohringer, V. S. Yakovlev, S. Zherebtsov, T. Pfeifer, A. M. Azzeer, M. F. Kling, S. R. Leone, and F. Krausz, Nature (London) **466**, 739 (2010).
[5] A. Wirth, M. Th. Hassan, I. Grguraš, J. Gagnon, A. Moulet, T. T. Luu, S. Pabst, R. Santra, Z. A. Alahmed, A. M. Azzeer,

V. S. Yakovlev, V. Pervak, F. Krausz, and E. Goulielmakis, Science **334**, 195 (2011).
[6] G. L. Yudin, S. Chelkowski, J. Itatani, A. D. Bandrauk, and P. B. Corkum, Phys. Rev. A **72**, 051401(R) (2005).
[7] A. D. Bandrauk, S. Chelkowski, P. B. Corkum, J. Manz, and G. L. Yudin, J. Phys. B **42**, 134001 (2009).
[8] S. Chelkowski, G. L. Yudin, and A. D. Bandrauk, J. Phys. B **39**, S409 (2006).
[9] G. L. Yudin, A. D. Bandrauk, and P. B. Corkum, Phys. Rev. Lett. **96**, 063002 (2006).
[10] E. A. Pronin, A. F. Starace, M. V. Frolov, and N. L. Manakov, Phys. Rev. A **80**, 063403 (2009).
[11] L. Y. Peng, E. A. Pronin, and A. F. Starace, New J. Phys. **10**, 025030 (2008).
[12] L. Roso-Franco, A. Sanpera, M. Ll. Pons, and L. Plaja, Phys. Rev. A **44**, 4652 (1991).
[13] S. C. Rae, X. Chen, and K. Burnett, Phys. Rev. A **50**, 1946 (1994).
[14] E. S. Smyth, J. S. Parker, and K. T. Taylor, Comput. Phys. Commun. **114**, 1 (1998).
[15] A. Castro, M. A. L. Marques, and A. Rubio, J. Chem. Phys. **121**, 3425 (2004).
[16] T. J. Park and J. C. Light, J. Chem. Phys. **85**, 5870 (1986).
[17] E. Cormier and P. Lambropoulos, J. Phys. B **30**, 77 (1997).
[18] D. A. Telnov and S.-I. Chu, Phys. Rev. A **83**, 063406 (2011).